

AN EMPIRICAL METHOD FOR IMPROVING THE QUALITY OF *RXTE* PCA SPECTRA

JAVIER GARCÍA¹, JEFFREY E. MCCLINTOCK¹, JAMES F. STEINER¹, RONALD A. REMILLARD², VICTORIA GRINBERG²
Draft version February 29, 2024

ABSTRACT

We fitted all of the several hundred *RXTE* PCA spectra of the Crab individually to a simple power-law model; the total number of counts in the composite spectrum is $> 10^9$. We then used the spectrum of residuals to derive a calibration tool, called `pcacorr`, that we apply to large samples of spectra for GX 339–4, H1743–322, and XTE J1550–564. Application of the tool improved the quality of all the fits, and the improvement is dramatic for spectra with $\gtrsim 10^7$ counts. The Crab residual spectrum is somewhat different for each of the five PCA detectors, but it was relatively stable over the course of the mission. We recommend that `pcacorr` be routinely applied to spectra with $\gtrsim 10^6$ counts and that one include a systematic error of 0.1%, rather than the 0.5–1% value that has customarily been used. We expect that application of the tool will result in an increase in sensitivity of the PCA to faint spectral features by up to an order of magnitude.

Subject headings: instrumentation: detectors – space vehicles: instruments – X-ray: individual (Crab, GX 339–4, H1743–322, XTE J1550–564)

1. INTRODUCTION

The Rossi X-ray Timing Explorer (*RXTE*), launched on 30 December 1995 and decommissioned on 4 January 2012, observed hundreds of X-ray sources during its 16 year lifetime. *RXTE* carried three instruments: The All Sky Monitor (ASM; Levine et al. 1996), consisting of three scanning detectors that surveyed essentially the full sky during each orbit (~ 93 min); the High Energy X-ray Timing Experiment (HEXTE; Rothschild et al. 1998), two clusters of phoswich scintillation detectors sensitive over the energy range 15–250 keV; and the Proportional Counter Array (PCA), a set of five xenon-gas proportional counters with a total effective area of 6500 cm² sensitive over the 2–60 keV energy range.

The PCA was the principal instrument aboard *RXTE*. Over the course of the mission, the PCA made $\approx 110,000$ pointed observations, each with a typical duration of a few thousand seconds; the total effective observation time for the mission was ≈ 295 Msec. This paper describes and makes readily available a new methodology for improving the quality of PCA spectra. Specifically, we recalibrate the detector response using a mission-averaged spectrum of the Crab Nebula.

The PCA was comprised of five nearly-identical Proportional Counter Units (PCUs), each with an effective area of 1600 cm². The PCA offered superb timing capability ($\Delta t \approx 1 \mu\text{s}$) and modest spectral resolution ($\sim 18\%$ at 6 keV). Moreover, the stability and predictability of the relatively low background (2 mCrab) allowed the PCA to explore the behaviors of a great variety of X-ray sources (e.g., Kaaret et al. 2004; Swank 1999, 2006). Details on the technical specifications, performance, and calibration of the PCA are available in Glasser et al. (1994); Zhang et al. (1993); Jahoda et al. (1996, 2006); Shaposhnikov et al. (2012).

Jahoda et al. (2006) describe the response of the PCA from the beginning of the mission until 2004. They showed that for

many observations the energy calibration of the instrument is limited by systematic errors below 10 keV. Specifically, they reported that the unmodeled variations in the instrumental background are less than 2% of the *observed* background below 10 keV and less than 1% in the 10–20 keV region. They therefore advocated a general and conservative approach of including an allowance for systematic error. Thereafter, it became standard practice in reducing/analyzing PCA spectra to add in each pulse height channel a systematic error of 0.5–1% in quadrature with the statistical error to mask the uncertainties in the model of the detector response. Assuming a competent spectral model of a source in question, this procedure allows one to achieve good fits.

The *RXTE* team later revised the PCA calibration, producing an updated physical model for the instrumental response. These efforts are fully described in Shaposhnikov et al. (2012), including the latest version of the response generator (`pcarmf v11.7`) and the channel-to-energy conversion table (`e05v04`). The new calibration, which was tested on the whole archive of observations for the Crab, showed a great improvement in performance with respect to earlier calibrations. Concerning systematic error, Shaposhnikov et al. (2012) recommended: “For most observations, the systematic error of 0.5% is sufficient, while for extreme cases it can be raised to 1.5%”³.

In this paper we go one step further in improving the calibration of the PCA. We combine several hundred spectra of the Crab accumulated over the lifetime of the mission to produce a single spectrum of residuals (data/model), which we describe in Section 2 and refer to throughout as a “ratio spectrum.” This ratio spectrum has the extreme statistical precision expected for an analysis based on $> 10^9$ source counts. We show that in fitting any PCA spectrum with $\gtrsim 10^6$ counts one can significantly reduce the effects of systematic errors due to uncertainties in the standard detector response files by simply dividing the observed counts by our ratio spectrum.

In Section 2 we compute a ratio spectrum, and in Section 4

¹ Harvard-Smithsonian Center for Astrophysics, 60 Garden St., Cambridge, MA 02138 USA; javier@head.cfa.harvard.edu, jem@cfa.harvard.edu, jsteiner@head.cfa.harvard.edu

² MIT Kavli Institute for Astrophysics and Space Research, MIT, 70 Vassar Street, Cambridge, MA 02139, USA; rr@space.mit.edu, grinberg@space.mit.edu

³ For a discussion of how systematic error affects confidence intervals, see Wilms et al. (2006), and for a thoughtful analysis on treating systematic error, including practical recommendations, see Hanke (2011).

we obtain, via an iterative procedure, a sequence of ratio spectra that quickly converges to our final product, which we refer to as a “correction curve.” We compute a correction curve for each individual PCU for each of the two principal gain intervals. Throughout, we refer to the complete suite of correction spectra, plus a Python script for correcting any PCA spectrum of interest, as the tool `pcacorr` (see Section 10). We demonstrate the performance of `pcacorr` by fitting selected spectra of GX 339–4, H1743–322, and XTE J1550–564 (Section 6), as well as spectra of the Crab itself (Section 5).

The tool `pcacorr` allows one to correct a PCA spectrum of a bright source of interest and achieve an acceptable fit to a model using a significantly lower level of systematic error. Our analysis indicates that the level of required systematics after the correction is applied is roughly 0.1%, rather than the standard prescription of 0.5–1%. Thus, application of the tool greatly increases the detection sensitivity of the PCA. The benefits are obvious. For example, key physical parameters may be more accurately and precisely determined. Additionally, and despite the limited energy resolution of the PCA, the greater sensitivity will likely enable the detection of subtle and previously undiscovered spectral features, such as photoelectric edges in disk-photospheric spectra (Kubota et al. 2010), or absorption lines in disk-wind spectra (e.g. Neilsen et al. 2012).

The paper is organized as follows. In the following section we present our analysis of the complete collection of archived PCA spectra of the Crab. Our method for correcting any PCA spectrum of interest is described in Sections 3 and 4. In Section 5 we first apply the method to individual Crab spectra, and in Section 6 we extensively apply the method to many spectra of three black hole binaries. In Sections 7–9 we examine in turn how the correction differs among the five PCUs, the stability of the correction over the mission lifetime, and how the correction depends on whether one considers a single detector layer or all three. We close with a discussion and our conclusions in Section 10.

2. FITS TO THE CRAB DATA AND THE CREATION OF A RATIO SPECTRUM

We have fitted all the archived spectra of the Crab taken with the PCA. The data for all five PCUs were reduced and background subtracted following procedures described more fully in McClintock et al. (2006). Briefly, the event files and spectra were screened using the data reduction tools from HEASOFT version 6.13. Data were taken in the “Standard 2 mode,” which delivers a PCA spectrum every 16 s. The bulk of the paper is focused on spectra created by summing the counts detected in all three gas layers of each PCU, although we have also analyzed all the Crab data for the top layer only (see Section 9). Background spectra were obtained using version 3.8 of the tool `pcabackest`, along with a background model `pca_bkgd_cmvle_eMv20111129.mdl`, which was provided by the PCA team and yields improved background spectra for bright sources (C. Markwardt, private communication). Background spectra were subtracted from the total spectra using the tool `mathpha`. The response files were generated using the latest version of the response generator `pcarmf` (version 11.7) and energy-to-channel conversion table (version `e05v04`) described in Shaposhnikov et al. (2012). We disregard data collected during the first 108 days, which corresponds to $\approx 2\%$ of the mission lifetime (Gain Epochs 1 and 2) for which the calibration of the PCA is unreliable.

A normalization correction for detector dead time was not applied to the data presented here (the typical correction factor was ≈ 1.05 , with extreme values of 1.019 and 1.069). Given our concern in this paper with systematic errors, we note that energy-dependent deadtime effects can in principle occur for bright sources because the source and background components are generally not corrected for deadtime in a self-consistent manner. For the Crab Nebula, where the deadtime is moderate and the source dominates the background out to 45 keV, we find that energy-dependent deadtime effects do not appear to be important and that they are unrelated to the sharp spectral features that are our concern in this paper. However, as a general caution, we note that significant systematic errors may arise in the analysis of soft broadband spectra of very bright sources from an inconsistent treatment of deadtime effects.

To bring focus to the paper, we primarily discuss and present results for the 554 spectra taken with PCU-2, the detector generally considered to be the best-calibrated and the one most often in operation. The time boundaries for the 554 archived spectra are associated with the time intervals of PCA FITS files (FS4a*) for data collected in the Standard-2 mode. However, we have analyzed all the PCA spectra of the Crab, and the `pcacorr` tool can be applied to a spectrum obtained by any one of the five PCUs. All of our data analysis is performed using the X-ray spectral fitting package XSPEC (Arnaud 1996), version 12.7.1. Thus, the criterion we rely on for goodness-of-fit in fitting models to data is

$$\chi^2 = \sum_k^N \frac{[S(k) - M(k)]^2}{\sigma^2(k)}, \quad (1)$$

where $S(k)$ and $M(k)$ are the source and model counts for channel k , respectively, and the summation is over all N channels. The squared error for channel k is

$$\sigma^2(k) = S(k) + B(k) + \sigma_{\text{sys}}^2(k), \quad (2)$$

where $B(k)$ is the background counts and $\sigma_{\text{sys}}^2(k)$ is the systematic error assumed for channel k . As a general rule, one expects that a good fit has been achieved when $\chi^2 \sim \nu$, where ν is the number of degrees of freedom, given by the number of channels minus the number of free fit parameters. Hence, it is customary to refer to the *reduced* $\chi^2_\nu \equiv \chi^2/\nu$, which has an expected value near unity if the data are well described by the model. While Equation 1 defines the goodness-of-fit statistic that is widely used in X-ray astronomy, several definitions of chi-squared are discussed in the literature that differ largely in how the errors in Equation 2 are estimated (e.g., see Section 7.4 in Feigelson & Babu 2012).

Because our goal is to assess systematic errors and improve the calibration of the detectors, we do *not* follow the standard practice of including an allowance for systematic errors in fitting spectra; we consider only the errors due to counting statistics (i.e., $\sigma_{\text{sys}}^2(k) = 0$), except where otherwise specified. Following Shaposhnikov et al. (2012), we ignored the unreliable data in channels 1–4, and noticed energies up to 45 keV. Each Crab spectrum is fitted to an absorbed power-law using `Tbabs*powerlaw` in XSPEC, assuming a fixed hydrogen column density of $N_{\text{H}} = 3.45 \times 10^{21} \text{ cm}^{-2}$. For the TBABS model (Wilms et al. 2000), we used the Anders & Grevesse (1989) set of solar abundances and the Balucinska-Church & McCammon (1992) cross sections. The resulting

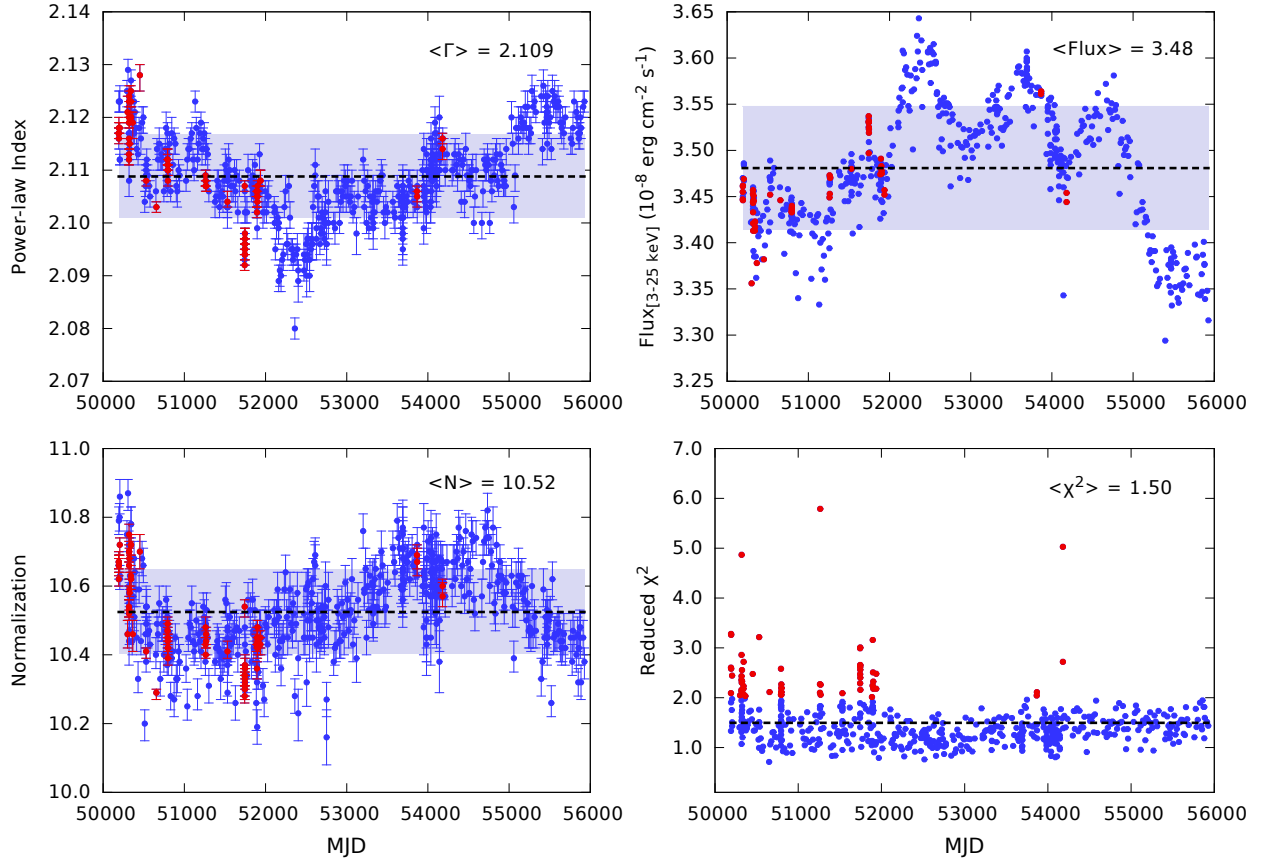


FIG. 1.— Results of fitting 554 PCU-2 spectra of the Crab to an absorbed power-law model with a fixed column depth of $N_{\text{H}} = 3.45 \times 10^{21} \text{ cm}^{-2}$. Panels show photon index, normalization, flux, and χ^2_{ν} resulting from the individual fits. Average values are marked with dashed lines and the shaded regions in the first three panels indicate their standard deviations. Data points in red correspond to fits with $\chi^2_{\nu} > 2$.

power-law indices, normalization, flux, and χ^2_{ν} for each fit are shown in Figure 1. Our results are similar to those shown in Shaposhnikov et al. (2012); specifically, the power-law index and power-law normalization display the same patterns of variability. The mean power-law index, normalization, flux, and reduced χ^2 for our complete sample are 2.11, 10.52, $3.48 \times 10^8 \text{ erg cm}^{-2} \text{ s}^{-1}$, and 1.50, respectively. The power-law index is consistent with that found by Shaposhnikov et al. (2012); however, our mean normalization is somewhat lower, likely because we do not correct the count rates for the effects of detector dead time, and our mean reduced χ^2 is slightly higher. The variations in flux follow closely those previously reported by Wilson-Hodge et al. (2011) who find that this variability is intrinsic to the Crab.

About 7% of the fits were relatively poor with $\chi^2_{\nu} > 2$; the corresponding data points in Figure 1 are shown in red. Despite the elevated values of χ^2_{ν} , the values of photon index and normalization are typical of the full data sample. The poorer fit quality is entirely due to longer exposure time, more counts, and hence the better statistical quality of the data. Figure 2 shows χ^2_{ν} versus the total number of counts for each observation. Most of the observations with $\chi^2_{\nu} > 2$ (red symbols) have more than 5×10^6 counts.

Figure 3 shows a standard data-to-model ratio spectrum produced by combining the data counts and the model counts for all 554 fitted Crab spectra. The total data counts S from the source (i.e., excluding the background) and the model

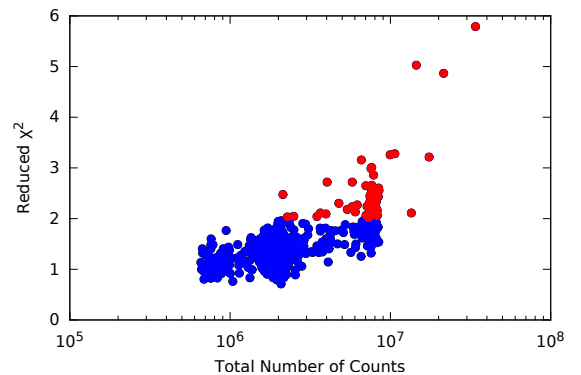


FIG. 2.— χ^2_{ν} as a function of total counts for the fits to all the 554 PCU-2 spectra of the Crab. Data points in red (which correspond to long exposures and many counts) indicate low-quality fits with $\chi^2_{\nu} > 2$.

counts are simply obtained by adding the net counts in each individual channel. A complication in combining the various spectra is that the energy assigned to each boundary is time-dependent, with discontinuous jumps at gain epoch boundaries and smooth evolution during a given epoch⁴. We deal with this problem by mapping all the individual spectra to the grid of energies of one of the spectra (the reference spectrum), which can be chosen at will; the ratio spectrum shown in Fig-

⁴ http://heasarc.gsfc.nasa.gov/docs/xte/e-c_table.html

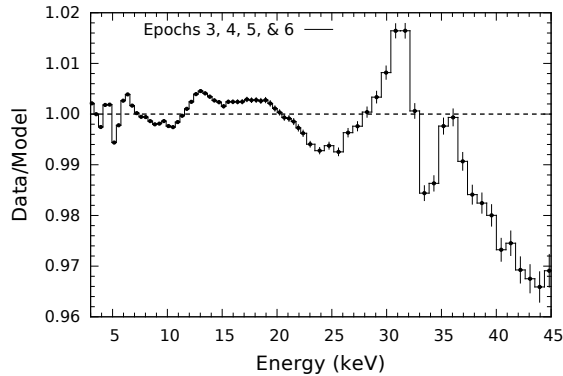


FIG. 3.— Ratio spectrum obtained by combining all 554 PCU-2 Crab spectra. This summation of 746 ks of Crab data, corresponding to 2×10^9 total counts, results in a ratio spectrum with extraordinary statistical precision.

Figure 3 was computed using the *RXTE* data set corresponding to obsID 60079-01-17-00. The mapping is accomplished via linear interpolation.

The error bars displayed in Figure 3 are given by the ratio of the square root of the total data counts D for each channel to the model counts (Equation 2). The combined ratio plot shown in Figure 3, which was computed using all 554 PCU-2 Crab spectra, is equivalent to what one would obtain by analyzing a single 746 ks Crab spectrum with 2×10^9 counts. The highly-significant features in the ratio spectrum (Figure 3) represent departures from the pure power-law spectrum expected for the Crab. By combining all the observations, we are able to sensitively probe the $\sim 1\%$ irregularities in the detector response, which have motivated observers over the years to include a typical allowance of $\sim 1\%$ for systematic errors when fitting PCA spectra (Section 1). Assuming that the synchrotron spectrum of the Crab is featureless and can be described by an unbroken power law, the irregularities are due to imperfections in the calibration of PCU-2. The ratio spectrum is fundamental to our method of significantly decreasing the level of systematic error in the data.

Possibly, the relatively sharp residual features shown in Figure 3 are unmodeled features associated respectively with the Xe L-edges known to be present at 4.78, 5.10, and 5.45 keV, and the Xe K-edge at 34.5 keV (Jahoda et al. 2006). Additionally, at energies above ~ 30 keV the spectrum generally trends downward, implying that the best-fit power law overpredicts the observed spectrum by $\approx 3\%$ at 45 keV. It is not clear whether this effect is instrumental or whether the Crab spectrum actually steepens. It is well-known that the spectrum of the Crab is a composite of nebular and pulsar components and that it breaks at ~ 100 keV (e.g., Strickman et al. 1979; Jung 1989; Yamada et al. 2011). Possibly, the Crab spectrum softens slightly in the PCA band, which would imply a gradual softening of the spectrum over a wide range of energies (Jourdain & Roques 2009) as opposed to an abrupt cutoff at ~ 100 keV. Alternatively, this downward trend above ~ 30 keV may be related to errors in the response files. That the effect is less significant in the ratio spectrum computed for the top xenon layer only (see Section 9) supports this hypothesis.

3. DEALING WITH CHANGING GAIN

As mentioned in Section 2 and illustrated in Figure 4, the gain of the PCUs changed continuously throughout the mission, while discontinuous changes occurred at the boundaries

between gain epochs. The constantly changing gain of a detector requires that each of the Crab spectra are mapped to a common reference grid of energies. As we show in Section 8, this procedure works well in delivering a stable and useful ratio spectrum within a particular gain epoch. However, as shown below, the ratio spectrum is not stable across the major boundary between Gain Epoch 3 and Gain Epoch 4 (which we refer to hereafter as Gain Epochs 4–6⁵) because the channel-to-energy assignments changed quite significantly. The gain discontinuity at this boundary is most problematic for the low-energy channels ($E \lesssim 7$ keV) whose statistical precision is extreme.

Instead of mapping all spectra to the grid of energies of one particular spectrum, as we did in Section 2, we now create a synthetic, high-resolution reference energy grid (similar to the E_p space used in Jahoda et al. 2006). Compared to the histogram (Figure 3), this new approach provides a ratio spectrum that resolves finer details and reduces interpolation errors. We choose a grid that encompasses all possible energy shifts in the channel boundaries occurring over the mission lifetime. The grid of 10^4 bins is homogeneous and covers the energy range 1–150 keV. Each individual spectrum is mapped to the grid by linear interpolation. Figure 5 shows the finely-gridded ratio spectrum resulting from the combination of all PCU-2 Crab spectra for Gain Epoch 4–6.

4. CORRECTION CURVES FOR THE TWO PRINCIPAL GAIN EPOCHS

At this point one could adopt the ratio spectrum shown in Figure 5 as a final product to be used in correcting all PCU-2 spectra obtained during Gain Epochs 4–6. However, via an iterative procedure we obtain a final product of much higher quality for use in correcting PCA spectra that we refer to hereafter as a “correction curve.” We now describe the iterative procedure and the creation of the correction curve.

The blue curve in Figure 6 (labeled iter 0) shows the same ratio spectrum plotted in Figure 5, but with the error bars suppressed for clarity. In the top two panels, this ratio spectrum is plotted in two separate energy intervals, 1–4 keV and 4–45 keV, because of the very different scale of the residuals. We perform the first iteration by dividing the counts in each of the 417 PCU-2 Crab spectra by the corresponding value given in the ratio spectrum shown in blue and labeled “iter 0” in Figure 6. In this way we produce a new ratio spectrum plotted in orange (iter 1) with the instrumental residuals now reduced to a level of $\sim 0.2\%$. Correcting the Crab spectra a second time using this ratio spectrum again further reduces the amplitudes of the residual features. After nine iterations, the residuals have been reduced to the extraordinary level of 0.05% for most channels (Figure 6).

Although the residuals are largest for the low-energy channels, the improvement is most dramatic for these channels because the data/model ratio was initially ~ 3.5 (top-left panel of Figure 6). However, in computing the original ratio spectrum (iter 0), we ignored channels 1–4 so that the correction at low energies is based on an extrapolation. Although the correction procedure dramatically reduces the residuals in these channels, the calibration is highly uncertain and is a topic for future study. We further note that, likewise, the extrapolation of the correction to energies above the 45 keV limit of our

⁵ We ignore the relatively unimportant changes at the boundaries between Gain Epochs 4 and 5 and Gain Epochs 5 and 6, which affected in each case only an individual detector (see Figure 4.)

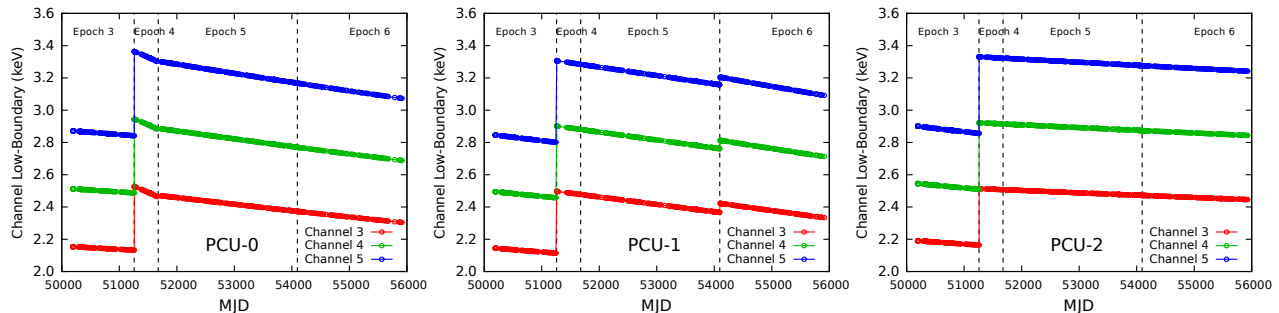


FIG. 4.— Variation of the energy of the lower boundary of channels 3, 4, and 5 during the 16-years of the *RXTE* mission (excluding Gain Epochs 1 and 2). The data correspond to the hundreds of Crab spectra taken with PCU-0 (left), PCU-1 (middle), and with PCU-2 (right). The vertical lines show the transitions between gain epochs. There are clear and abrupt changes in the channel energies for all five PCUs in passing from Epoch 3 to Epoch 4, which occurred on MJD 51259. The transitions between Epoch 4 and Epoch 5, and between Epoch 5 and Epoch 6, only affected PCU-0 and PCU-1, respectively; the effect on the channel boundaries of these detectors is small and we ignore them.

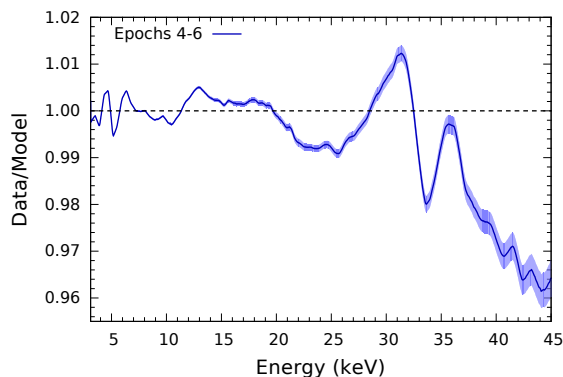


FIG. 5.— Ratio spectrum comparable to the one shown in Figure 3 but computed using a high-resolution grid and for Gain Epochs 4–6 only. The lighter shaded region shows the level of the statistical error.

fits, and over the entire energy range of the PCA, also seems to perform well. The behavior of the correction for channels 1–4 and for $E > 45$ keV is beyond the scope of this paper and will not be discussed further.

The flow diagram shown in Figure 7 summarizes the entire process employed in producing the final correction curve. The individual Crab spectra in the set of observations S_j^i are identified by the index j , while the index i is the iteration number. It is important to emphasize that the ratio spectra R^i are used at each iteration step i to correct the current set of corrected observations S_j^i ; i.e., R^i at each step is *not* used to correct the original uncorrected data S_j^0 . Thus, as consecutive iterations are performed, the magnitude of the correction decreases and successive ratio spectra approach unity, as illustrated in Figure 6. By visual inspection, we determined that after nine iterations the changes in the ratio spectra were negligible (thus, $\text{imax}=9$). Notice that because the corrected set of spectra after i iterations is

$$S_j^{i+1} = \frac{S_j^i}{R^i}, \quad (3)$$

then

$$S_j^{i+1} = \frac{S_j^{i-1}}{R^i R^{i-1}} = \frac{S_j^0}{R^i R^{i-1} \dots R^0}, \quad (4)$$

and one can write a *final correction curve* as

$$C = \prod_i^{\text{imax}} R^i. \quad (5)$$

Denoting S_j^\dagger as the final set of corrected Crab spectra after imax iterations, then the curve C can be used to directly correct any set of source spectra S_j^0 simply by

$$S_j^\dagger = \frac{S_j^0}{C}. \quad (6)$$

The final correction curve C , while derived using the Crab, can be applied to all sources, i.e., it provides a detailed description of the instrument response itself, and it is applicable to a PCA spectrum X_j^0 of any object (including the Crab). In fact, a suite of 20 such universal corrections curves are computed, one for each PCU, gain epoch, and detector configuration (see Section 10).

The final correction curve for PCU-2, which can be used to correct the spectrum of any source observed during Gain Epoch 4–6, is shown in the right panel of Figure 8. Because of the abrupt change in the channel boundaries between Gain Epoch 3 and Gain Epochs 4–6, we have produced a pair of correction curves for each PCU; the correction curve for PCU-2 for Gain Epoch 3 is shown in the left panel of Figure 8. Meanwhile, we ignore the boundaries between Gain Epochs 4 and 5, and between Gain Epochs 5 and 6, because they are relevant only for PCU-0 and PCU-1 (which lost their propane layers), and these discontinuities are weak and do not affect our results.

The pair of correction curves shown in Figure 8 are of central importance in the rest of the paper. While the curves are quite dissimilar at energies $\lesssim 7$ keV, they are qualitatively similar at energies above ~ 7 keV; e.g., both spectra show a prominent peak near 30 keV and a downward trend above that energy. The Epoch 3 and Epochs 4–6 correction curves (Figure 8) were computed using 137 and 417 Crab spectra, and the duration of each was 18% (2.9 yrs) and 80% (12.8 yrs) of the mission lifetime, respectively. Meanwhile, we ignore the data for Gain Epochs 1 and 2 (2% of the mission lifetime) because the calibration of the detectors is uncertain.

Instead of correcting the spectrum, we could have equivalently chosen to correct the response file. We chose to correct the spectrum because the makeup of response files prepared by different observers can differ significantly (e.g., the observer may or may not choose to include the effective area in the response file). In the following two sections, we illustrate the use of the `pcacorr` tool by correcting PCU-2 spectra of the Crab and three black holes.

5. APPLYING `PCACORR` TO INDIVIDUAL CRAB SPECTRA

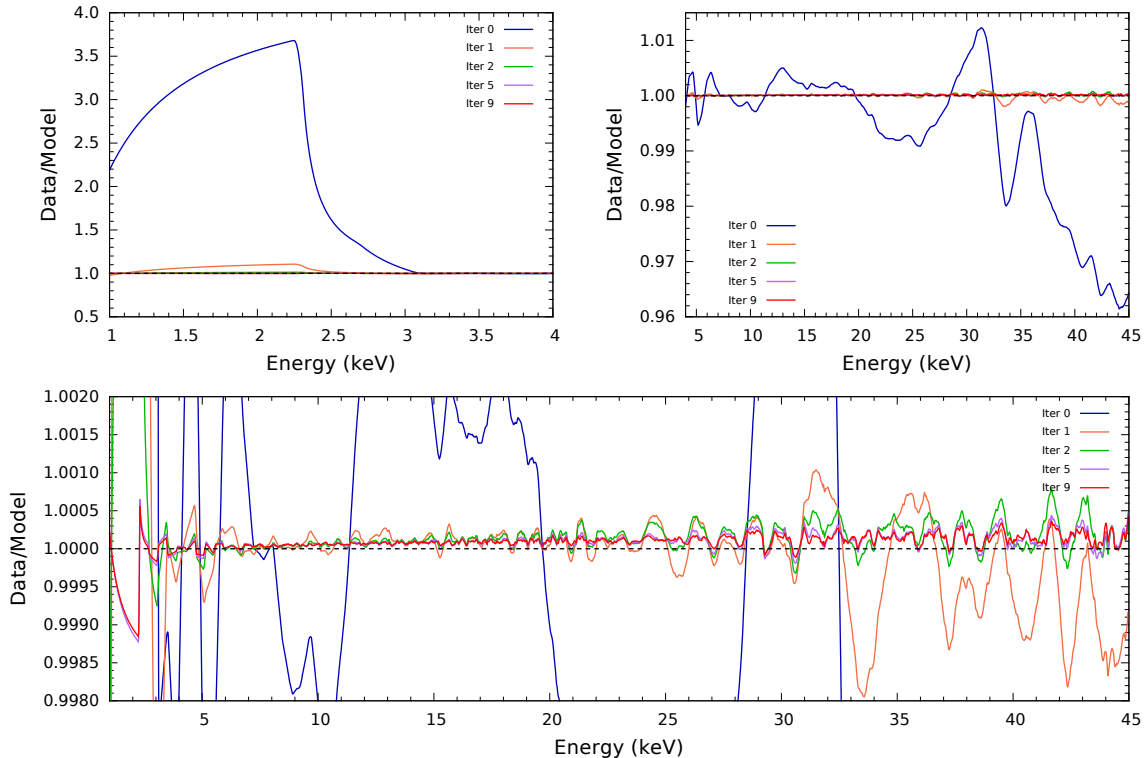


FIG. 6. — Top panels: Low-energy (left) and high-energy (right) spectral regions showing several ratio spectra obtained by combining 417 PCU-2 Crab spectra collected during Gain Epochs 4–6. The parent ratio spectrum labeled iter 0 (blue curve) is identical to that shown in Figure 5. The smaller-amplitude daughter spectra, which were computed using the iterative procedure described in the text, are sensitively displayed over the full 1–45 keV range in the lower panel. For most channels, nine iterations suffice to reduce the instrumental residuals to a level of $\sim 0.05\%$.

We now correct the 417 PCU-2 spectra of the Crab collected during Gain Epochs 4–6. For each Crab spectrum, we divide the counts in each channel, as well as the error, by the corresponding value of the correction curve shown in the right panel of Figure 8. We then fit both the corrected and uncorrected spectra to a simple power-law model precisely as described in Section 2, ignoring channels 1–4 and data above 45 keV. As before, and throughout this paper (apart from two minor exceptions, which are noted in the following paragraph and in the following section) we do not include any allowance for systematic errors when fitting the data. The values of χ^2_ν for the fits to the corrected and uncorrected spectra are compared in Figure 9.

In all cases, the correction improves the quality of the fit significantly, although the improvement is unremarkable for observations with fewer than $\sim 10^6$ counts. The mean values of the broadband model parameters (i.e., photon index, normalization, and flux) are essentially unchanged by the correction. The efficacy of the correction increases markedly with the number of counts. Despite the excellent performance of the `pcacorr` tool, there is still an upward trend in χ^2_ν with the number of counts and fits to the spectra with $\gtrsim 10^7$ counts can be improved further. As one of the minor exceptions mentioned above, we now make allowance for systematic error: Including a systematic error of 0.1%, we find that in almost all cases χ^2_ν decreases and that its values is now everywhere close to unity. The decrease is most obvious for the two longest exposure with $> 10^7$ counts. We therefore suggest that a 0.1% systematic error be routinely included when fitting PCA data that has been corrected using the `pcacorr` tool.

6. TESTING `PCACORR` ON SPECTRA OF STELLAR-MASS BLACK HOLES

In applying the `pcacorr` tool to the spectra of three well-studied black hole binaries, GX 339–4, H1743–322, and XTE J1550–564, we have two goals: To establish whether the residual features evident in the ratio spectrum (Figure 3) are indeed instrumental, and to test the effectiveness of the correction in improving fits to bright-source PCA spectra. As for the Crab spectra (Section 5), both the counts and the error at each channel in the source spectrum are divided by the respective value of the correction curve (while the errors in the latter are ignored).

We first test the tool using high-luminosity PCU-2 spectra of GX 339–4, specifically, the brightest 100 hard-state spectra (hardness > 0.75 ; see Remillard & McClintock 2006). These data were collected during Gain Epoch 5, and we therefore use the ratio spectrum shown in the right panel of Figure 8. We ignore channels 1–4 and channels above 45 keV and set the systematic uncertainty to zero. We again use a power-law model; however in this case, a smeared-edge (constrained to 7–9 keV) and a Gaussian line (constrained to 6–7 keV) are required to account for reflection features (which are not present in the Crab): `TBabs*smedge*(powerlaw+Gaussian)`. The model was fitted both to the original spectra and to the corrected spectra; the differences in χ^2 are shown in Figure 10. We find consistently better fits for the corrected data, with $\Delta\chi^2$ steadily decreasing as the number of counts increases, as expected.

In this example and the two that follow, as a simple check on the competency of the models we employ, we also fitted the

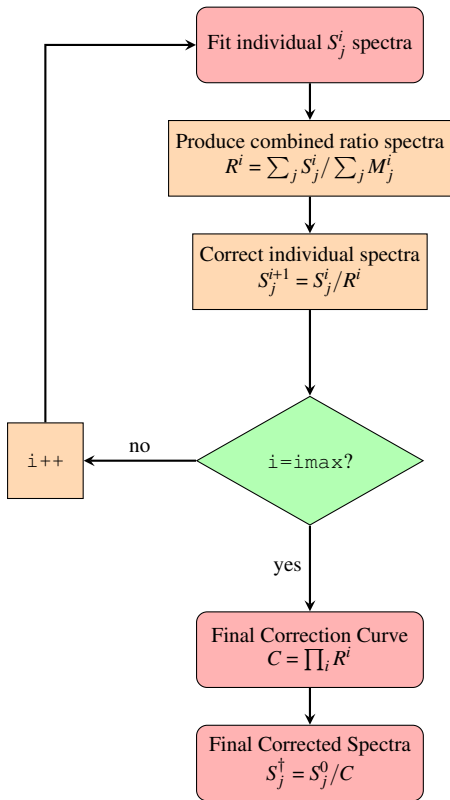


FIG. 7.— Flow diagram showing the process employed in producing a correction curve C using a collection of Crab spectra. The indices i and j denote the iteration number and the number of a particular spectrum, respectively. (For simplicity, we omit the use of a third and obvious index for channel number). Ratio spectra R^i computed for several iterations are shown in Figure 6, and the final correction curve C is shown in Figure 8.

same data sets using the standard past practice of including a systematic error of 1%; as expected, we obtained satisfactory fits with $\chi_\nu^2 \sim 1$. Here, and in Section 5 (where we derive our recommendation that 0.1% systematic error be routinely applied) are the only places in this paper where we include any allowance for systematic error.

A similar test was performed on the 100 brightest soft-state PCU-2 spectra of H1743–322. In the soft (or thermal) state, the source spectrum at low energies is dominated by the accretion-disk component. Accordingly, our simple model includes a multi-temperature disk component (while excluding the unnecessary reflection component): $\text{TBabs} * (\text{powerlaw} + \text{diskbb})$. Our procedures are otherwise identical to those used in fitting the spectra of GX 339–4 and the Crab. Figure 11 shows for each spectrum the improvement in χ^2 achieved by applying the correction. As in the case of GX 339–4, the benefit of applying the correction grows as the number of counts increases. The results summarized in Figures 10 and 11 clearly demonstrate the efficacy of the correction for both hard- and soft-state data, which indicates that the tool has broad applicability.

We have also tested the tool using Epoch 3 data, namely, 94 of the brightest soft-state spectra of XTE J1550–564. In this case, the relevant correction curve is the one shown in the left panel of Figure 8. The original and corrected data are fitted with the same model for the continuum used in fitting the spectra of H1743–322, except in this case we added a smeared Fe edge constrained to 7–9 keV:

$\text{Tbabs} * \text{smedge} (\text{powerlaw} + \text{diskbb})$. As shown in Figure 12, the results closely mirror those obtained for GX 339–4 and H1743–322.

Finally, we tested the correction using an advanced reflection model applied to a bright subset of the GX 339–4 hard-state spectra discussed above. Specifically, we selected 23 spectra with normalized PCU-2 count rates between 1000 and 1100 cts s^{-1} , which corresponds to an intensity of ~ 0.4 Crab. These spectra were obtained from consecutive observations performed between 2002-04-20 and 2002-04-30 (MJD 52384.126 to 52394.444). The model consists of an absorbed power law with exponential cutoff and a blurred X-ray reflection component. In this instance, we used the latest version of the relativistic reflection model RELXILL (García et al. 2014). The model is simply expressed as $\text{Tbabs} * \text{relxill}$, where RELXILL already includes the power-law component. Once again, a significant improvement is consistently obtained by applying the correction.

In considering how the parameters of our physically well-grounded reflection model are affected by making the correction, we have fitted the same 23 spectra simultaneously with all the parameters tied except for a normalization constant⁶. The correction significantly improved the composite fit, $\Delta\chi^2 = 313.04$; with no correction we obtained $\chi_\nu^2 = 1.91$, while with the correction we obtained $\chi_\nu^2 = 1.71$ (for 1605 degrees of freedom in both cases). As always, we do not include any allowance for systematic error, which contributes to the large values of χ_ν^2 . Our purpose here is not to perform a detailed analysis of these spectra, but rather to determine if the correction significantly affects the parameters of this detailed model.

Despite the large improvement in χ^2 , the model parameters are only slightly affected. In fact, the parameters that describe the continuum (e.g., photon index, ionization parameter, reflection fraction and normalization) are unaffected by the correction. The only parameters that are modestly affected are those informed by the reflection component, i.e., the inclination angle, inner-radius of the accretion disk, and Fe abundance. These are physically interesting model parameters which control the strength and shape of both the Fe K emission line at ~ 6.4 keV and the Fe K edge at ~ 7 keV. This is a particularly important result in the context of measuring the spins of black holes by the Fe-line method, which relies on accurate modeling of the profile of the Fe K emission line (e.g., Brenneman 2013).

7. COMPARING THE CORRECTION CURVES FOR THE FIVE PCUS

As discussed in Section 2, the channel boundaries change with time. In addition, the energy-to-channel conversion is different for each of the PCU detectors. Accordingly, one expects that if the features in the ratio spectra are attributable to unmodeled instrumental artifacts, they should differ between detectors. We have confirmed this expectation by repeating the process described in Section 4 for each of the PCUs. As before and for simplicity, we only show the results of combining observations taken during Gain Epochs 4–6. An overlay showing the correction curves for each detector is presented in Figure 13. Given that only a subset of the PCUs are used in a given observation, each unit has a different available exposure time and total counts. This information is summarized in Table 1.

⁶ This procedure is well motivated because the data are selected to have the same intensity and spectral hardness.

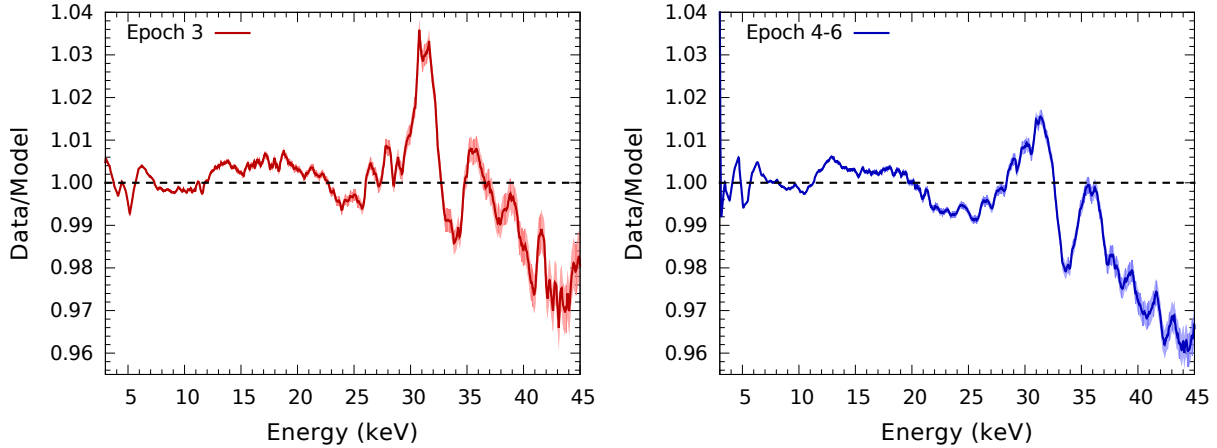


FIG. 8.— Our adopted PCU-2 correction curves, one for each of the two principal gain periods, computed using a high-resolution energy grid after 9 iterations (see Section 4). Left: Computed for 137 PCU-2 Crab spectra taken during Gain Epoch 3; equivalent to a 262 ks observation with 6×10^8 counts. Right: Computed for 417 PCU-2 spectra taken during Gain Epochs 4–6; equivalent to a 484 ks observation with 10^9 counts. The lighter shaded region bounding each curve shows the level of the statistical error.

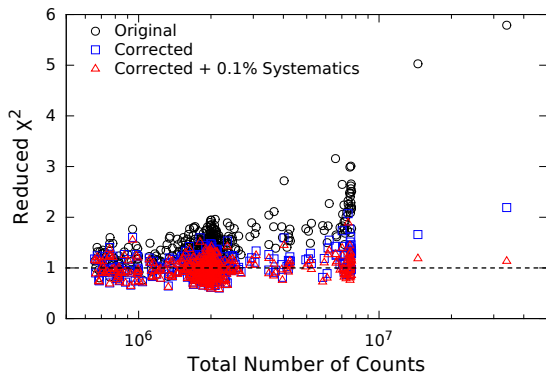


FIG. 9.— Goodness-of-fit (χ^2_{ν}) obtained for the 417 PCU-2 Crab observations taken during Gain Epochs 4–6. The model is an absorbed power-law (TBabs*powerlaw) with $N_{\text{H}} = 3.45 \times 10^{21} \text{ cm}^{-2}$. Black circles show χ^2_{ν} for the original spectra (like in Figure 2), while the blue squares are for the spectra that have been divided by the correction curve shown in the right panel of Figure 8. For the original and corrected data, the systematic uncertainty has been set to zero. Including a systematic error of 0.1% is sufficient to bring χ^2_{ν} to essentially unity for all corrected spectra (red triangles).

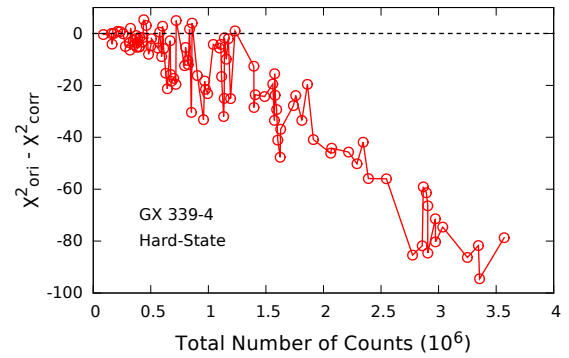


FIG. 10.— Improvement in χ^2 as a function of total counts for 100 high-luminosity spectra of GX 339-4 in the hard state. The principal component in the model is an absorbed power law; a Gaussian and a smeared edge were included as cosmetic components. Plotted is the difference in χ^2 between the original uncorrected spectra and their corrected counterparts. The data were corrected using the correction curve for Epochs 4–6 (right panel of Figure 8). All spectra were taken with PCU-2. Data for channels 1–4 and for energies above 45 keV are ignored. Systematic errors are set to zero.

TABLE 1
DETAILS OF THE CRAB OBSERVATIONS FOR GAIN
EPOCHS 4–6

PCU	No. of Spectra	Exposure Time (s)	No. of Counts (10^9)
0	373	447986	1.07
1	325	313936	0.73
2	417	483826	1.05
3	286	288336	0.64
4	329	316144	0.64

As shown in Figure 13, the correction curves of the five PCUs are quite similar in several respects. Notably, the most prominent features are present in all of the curves. For example, the narrow absorption feature near 34 keV (presumably due to the Xe K-edge) and the associated excess around 30–32 keV are pronounced for all the PCUs. Also, all of the curves

roll off at high energies, although the effect is significantly stronger for PCU-3. Meanwhile, there are significant differences: The corrections for PCU-1 deviates from the norm for energies in the range ~ 7 –20 keV. Of the two narrow absorption features seen in the correction for PCU-2 at ≈ 4.0 keV and ≈ 5.5 keV (right panel Figure 8), only the latter feature is common to all the PCUs (see the inset in Figure 13).

8. TEMPORAL STABILITY OF THE CORRECTION CURVES

Given that the instrument response changes gradually as the detectors age, and even suddenly, e.g., in the case of the loss of propane layers of PCU-0 (May, 2000) and PCU-1 (December, 2006), we have studied the stability of the correction over time. Here, we again discuss only our results for PCU-2, while noting that we have checked and found quite similar results for all the PCUs. Also, we consider only the stability of the correction curve for Gain Epochs 4–6 because it covers 80% of the mission. To assess stability, we have produced three additional correction curves by partitioning Epochs 4–6 with its 417 Crab observations into three sequential time

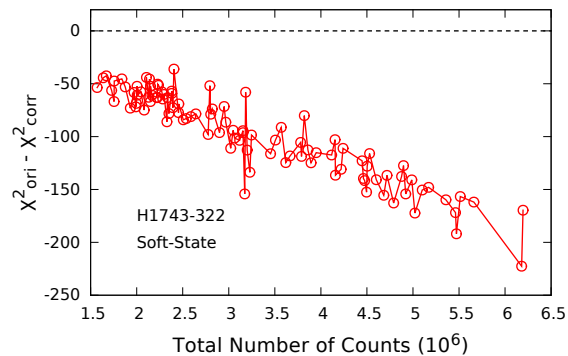


FIG. 11.— Improvement in χ^2 as a function of total counts for 100 high-luminosity spectra of H1743–322 in the soft state. The model consists of a multi-temperature disk component as well as an absorbed power-law component. The data were corrected using the correction curve for Epochs 4–6 (right panel of Figure 8). Data for channels 1–4 and for energies above 45 keV are ignored. Systematic errors are set to zero.

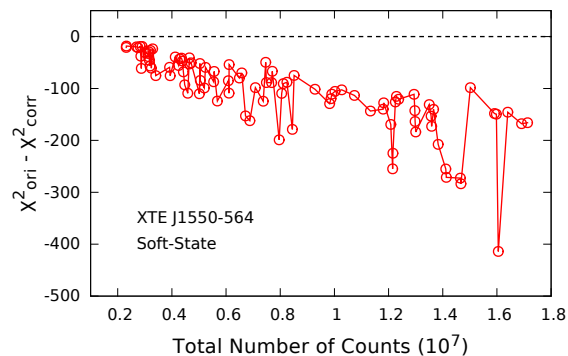


FIG. 12.— Improvement in χ^2 as a function of total counts for 94 high-luminosity spectra of XTE J1550–564 in the soft state. The model consists of a multi-temperature disk component and an absorbed power law plus a smeared edge. The data were corrected using the correction curve for Epoch 3 (left panel of Figure 8). All spectra were taken with PCU-2. Data for channels 1–4 and for energies above 45 keV are ignored. Systematic errors are set to zero.

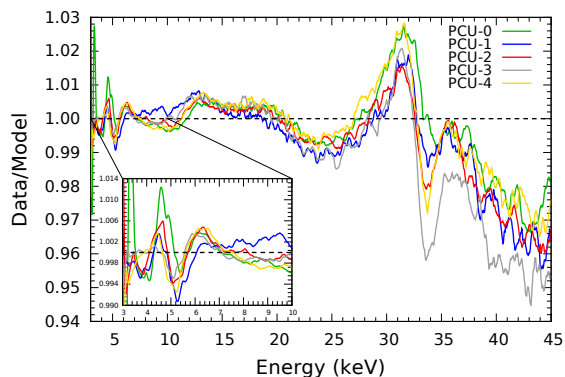


FIG. 13.— Correction curves for all five PCUs using only observations taken during Gain Epochs 4–6. For details on the input spectra, see Table 1.

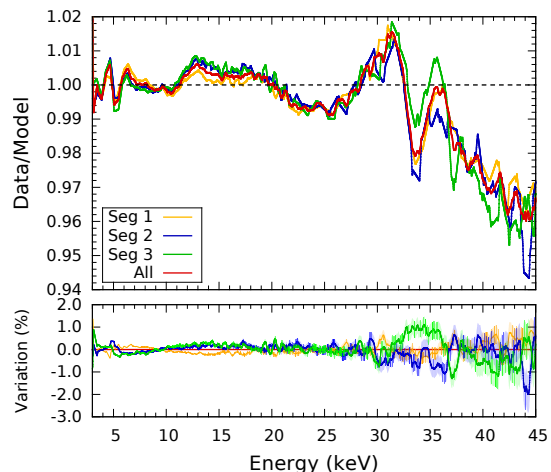


FIG. 14.— Top: Correction curves for PCU-2 in three sequential time intervals covering Gain Epochs 4–6. For comparison, the full correction curve for the entire period is also shown (red line). Bottom: The three individual correction spectra divided by the full correction curve. The statistical error for each curve is indicated by the width of the shaded region.

intervals, each containing 139 observations: (1) spectra obtained between 24 March 1999 and 26 September 2002 (MJD 51261–52543); (2) spectra obtained between 10 October 2002 through 17 November 2006 (MJD 52557–54056); and (3) spectra collected during the final phase of the mission, after 18 November 2006 (MJD 54057).

The correction curve for each time interval and an average over the entirety are compared in the upper panel of Figure 14. The lower panel of Figure 14 shows the percentage deviation of each segment with respect to the total correction curve (also shown in Figure 8). The correction curves produced for the three time intervals are very close to each other for most of the channels, with the most pronounced differences ($\sim 3\%$) at high energies where the statistical precision is relatively poor. We conclude that the response of a given PCU is stable over a gain epoch, which justifies using a single curve averaged over a gain epoch to correct a spectrum of interest.

9. CORRECTION CURVE FOR A SINGLE XENON LAYER

Each PCU is a three-layered detector. In reducing PCA data, one can select data either for all three layers combined or for the top layer only. All the results that we have presented so far are for the full three-layer detector. Meanwhile, we have also computed the single-layer correction for all the PCUs following exactly the same procedures described in Sections 2 and 4. The correction curve for PCU-2 for the top layer only is shown in Figure 15, where it is compared to the correction curve for all three layers. This latter correction is identical to the one that appears in the right panel of Figure 8. Both PCU-2 corrections were computed using the 417 Crab spectra collected during Gain Epochs 4–6.

There are significant differences between the two correction curves. Most notably, the roll off at high energies, which is present in the 3-layer correction of all of the PCUs (Figure 7), is less pronounced in the correction computed for a single layer; this is true for all the PCUs and is illustrated for PCU-2 in Figure 15. This difference suggests that the roll off in the 3-layer correction curve discussed in Section 2 is due to an error in the model of the detector response, rather than to a break in the spectrum of the Crab. Because the single-layer and 3-layer ratio spectra are distinctly different, we have com-

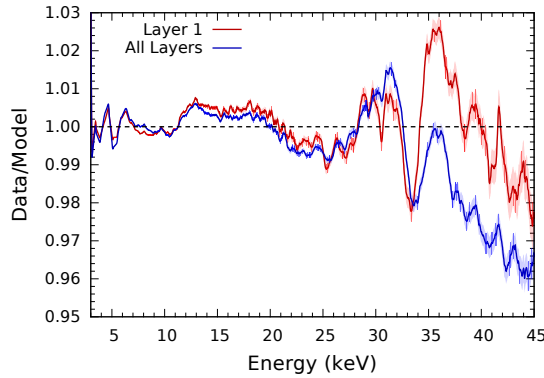


FIG. 15.— Correction curves derived using the 417 PCU-2 Crab spectra from Epochs 4–6. The blue spectrum was produced for the full 3-layer detector (the same curve shown in the right panel of Figure 8), while the red curve was produced for the top layer only. The lighter shaded region around each curve shows the level of the statistical error.

puted a total of 20 correction curves (2 detector configurations times 2 gain epochs times 5 PCUs).

10. DISCUSSION AND CONCLUSIONS

A precise physical interpretation of the residual features seen in the correction curves (Figures 8, 13, and 15) is beyond the scope of this paper. Nevertheless, we identify and comment on three possible origins of these features, namely, that they are: (i) intrinsic to the Crab; (ii) imperfectly-modeled instrumental features due, e.g., to the Xe L- and K-edges; or (iii) produced by inaccuracies in defining the channel boundaries. The first two possibilities are expected to produce features common to all the PCUs, while the latter is expected to produce narrow features that differ among the PCUs because the gains of the individual detectors differ.

The hypothesis (i) that the discrete features in the ratio spectra are present in the spectrum of the Crab is disfavored because of our success in correcting the spectra of GX 339–4, H1743–322, and XTE J1550–564; furthermore, such features are not expected to be present in the synchrotron spectrum of the Crab. However, as discussed in Section 2, the gradual roll off of the 3-layer correction curve at energies $\gtrsim 20$ keV may be attributable to a break in the spectrum of the Crab.

Hypothesis (ii) is favored by the many remarkably similar features that appear in the correction curves of the five PCUs (Figure 13), which strongly indicates that the features are instrumental. Below ~ 7 keV, however, there are narrow features in the correction curves that vary from PCU to PCU (see Section 7); these discordant features favor hypothesis (iii), indicating that the energies assigned to the channel boundaries are inaccurate.

Regardless of the cause of the features, we have demonstrated that one can use spectra of the Crab to routinely and significantly reduce systematic error and improve the quality of PCA spectra; the results are dramatic for high signal-to-noise data, with increases in sensitivity to faint spectral features for bright sources by up to an order of magnitude. As we have shown, the method works regardless of spectral shape, e.g., whether the object spectrum is thermal and soft or whether it is dominated by a hard power law. Furthermore, using a sophisticated reflection model and a homogeneous sample of hard-state spectra of GX 339–4, we found only modest changes in some of the parameters, namely, those tied to the reflection features (such as inclination and inner-disk radius). Meanwhile, the model parameters that determine the continuum were unaffected.

In summary, by analyzing more than 1 billion counts at once we have sensitively detected faint residual features in global spectra of the Crab Nebula. As we have demonstrated, using the `pcacorr` tool to correct an arbitrary object spectrum with $\gtrsim 10^6$ counts significantly improves the quality of the fit. We have also demonstrated that the inclusion of systematic uncertainty at the level of 0.1% is sufficient to achieve acceptable fits ($\chi^2_\nu \sim 1$; Figure 9), and we recommend routine use of 0.1% systematic error when analyzing PCA data that have been corrected with the present tool. Following a period of further testing of `pcacorr` on a wider range of black-hole and neutron-star spectra, a Python script that automates the correction of any PCA spectrum of interest, along with a complete set of 20 correction curves (2 detector configurations times 2 sets of gain epoch times 5 PCUs) will be made publicly available at <http://hea-www.cfa.harvard.edu/javier/pcacorr/>.

JG and JEM acknowledge the support of NASA grant NNX11AD08G. JFS has been supported by NASA Hubble Fellowship grant HST-HF-51315.01. VG acknowledges support provided by NASA through the Smithsonian Astrophysical Observatory (SAO) contract SV3-73016 to MIT for support of the Chandra X-Ray Center (CXC) and Science Instruments; CXC is operated by SAO for and on behalf of NASA under contract NAS8-03060. We thank the anonymous referee for a careful reading of our paper, thoughtful criticisms and useful suggestions. We also thank Jörn Wilms, Keith Jahoda, Craig Markwardt, and Nikolai Shaposhnikov for useful suggestions and valuable discussions.

REFERENCES

- Anders, E., & Grevesse, N. 1989, *Geochim. Cosmochim. Acta*, 53, 197
- Arnaud, K. A. 1996, in *Astronomical Society of the Pacific Conference Series*, Vol. 101, *Astronomical Data Analysis Software and Systems V*, ed. G. H. Jacoby & J. Barnes, 17
- Balucinska-Church, M., & McCammon, D. 1992, *ApJ*, 400, 699
- Brenneman, L. 2013, *Measuring the Angular Momentum of Supermassive Black Holes*
- Feigelson, E. D., & Babu, G. J. 2012, *Modern Statistical Methods for Astronomy*
- García, J., et al. 2014, *ApJ*, 782, 76
- Glasser, C. A., Odell, C. E., & Seufert, S. E. 1994, *IEEE Transactions on Nuclear Science*, 41, 1343
- Hanke, M. 2011, PhD thesis, Dr. Karl Remeis-Sternwarte, Astronomisches Institut der Universität Erlangen-Nürnberg, Sternwartstr. 7, 96049 Bamberg, Germany
- Jahoda, K., Markwardt, C. B., Radeva, Y., Rots, A. H., Stark, M. J., Swank, J. H., Strohmayer, T. E., & Zhang, W. 2006, *ApJS*, 163, 401
- Jahoda, K., Swank, J. H., Giles, A. B., Stark, M. J., Strohmayer, T., Zhang, W., & Morgan, E. H. 1996, in *Society of Photo-Optical Instrumentation Engineers (SPIE) Conference Series*, Vol. 2808, *EUV, X-Ray, and Gamma-Ray Instrumentation for Astronomy VII*, ed. O. H. Siegmund & M. A. Gummin, 59–70
- Jourdain, E., & Roques, J. P. 2009, *ApJ*, 704, 17
- Jung, G. V. 1989, *ApJ*, 338, 972

- Kaaret, P., Lamb, F. K., & Swank, J. H., eds. 2004, American Institute of Physics Conference Series, Vol. 714, X-Ray Timing 2003: Rossi and Beyond
- Kubota, A., Done, C., Davis, S. W., Dotani, T., Mizuno, T., & Ueda, Y. 2010, *ApJ*, 714, 860
- Levine, A. M., Bradt, H., Cui, W., Jernigan, J. G., Morgan, E. H., Remillard, R., Shirey, R. E., & Smith, D. A. 1996, *ApJ*, 469, L33
- McClintock, J. E., Shafee, R., Narayan, R., Remillard, R. A., Davis, S. W., & Li, L.-X. 2006, *ApJ*, 652, 518
- Neilsen, J., Petschek, A. J., & Lee, J. C. 2012, *MNRAS*, 421, 502
- Remillard, R. A., & McClintock, J. E. 2006, *ARA&A*, 44, 49
- Rothschild, R. E., et al. 1998, *ApJ*, 496, 538
- Shaposhnikov, N., Jahoda, K., Markwardt, C., Swank, J., & Strohmayer, T. 2012, *ApJ*, 757, 159
- Strickman, M. S., Johnson, W. N., & Kurfess, J. D. 1979, *ApJ*, 230, L15
- Swank, J. H. 1999, *Nuclear Physics B Proceedings Supplements*, 69, 12
- . 2006, *Advances in Space Research*, 38, 2959
- Wilms, J., Allen, A., & McCray, R. 2000, *ApJ*, 542, 914
- Wilms, J., Nowak, M. A., Pottschmidt, K., Pooley, G. G., & Fritz, S. 2006, *A&A*, 447, 245
- Wilson-Hodge, C. A., et al. 2011, *ApJ*, 727, L40
- Yamada, S., et al. 2011, *PASJ*, 63, 645
- Zhang, W., Giles, A. B., Jahoda, K., Soong, Y., Swank, J. H., & Morgan, E. H. 1993, in *Society of Photo-Optical Instrumentation Engineers (SPIE) Conference Series*, Vol. 2006, EUV, X-Ray, and Gamma-Ray Instrumentation for Astronomy IV, ed. O. H. Siegmund, 324–333